INSTITUTE OF PHYSICS PUBLISHING JOURNAL OF PHYSICS B: ATOMIC, MOLECULAR AND OPTICAL PHYSICS

J. Phys. B: At. Mol. Opt. Phys. **34** (2001) 4041–4052 PII: S0953-4075(01)26632-2

Electron collisions with OClO using the *R*-matrix method

K L Baluja[1], **N J Mason, L A Morgan and Jonathan Tennyson**

Department of Physics and Astronomy, University College London, Gower Street, London WC1E 6BT, UK

Received 5 July 2001, in final form 23 August 2001
Published 5 October 2001
Online at stacks.iop.org/JPhysB/34/4041

Abstract

The *R*-matrix method is used to calculate elastic and excitation cross sections of four low-lying electronic states of the OClO molecule, designated as the X $^2B_1$, 1 $^2A_1$, 1 $^2B_2$ and 1 $^2A_2$ states. Eight states, four doublets and four quartets are included in the close-coupled expansion; these excited states are predicted to have vertical excitation energies in the range 2.956–8.206 eV, in fair agreement with published multireference configuration-interaction calculations. The experimentally determined excitation energy of the atmospherically most important state 1 $^2A_2$ centred around 3.5 eV is in excellent agreement with our value of 3.44 eV. A bound state of $OClO^-$ with $^1A_1$ symmetry with an adiabatic electron affinity of 1.558 eV at equilibrium geometry of OClO is found. There is a shape resonance of $^3B_1$ symmetry at 2.96 eV and higher-lying shape resonances of $^1B_1$, $^1A_2$ and $^3A_2$ symmetries located at 5.75, 8.06 and 7.22 eV, respectively. All the resonances are rather broad. The resonance positions correlate well with the maxima found in dissociative electron attachment cross section measurements. Rotationally inelastic scattering cross sections are compared with experiment and there is very good agreement for electron energies above 100 meV. Excitation cross sections for three excited states are presented for electron-impact energies up to 10 eV. Total integral cross sections are also compared with experiment.

1. Introduction

It is now well established that depletion of the ozone layer occurs during springtime in the stratospheric polar vortex above Antarctica (Cicerone 1987, Rowland 1991). The ozone-destroying reaction cycles involve reactive halogen free radicals whose main sources are chlorofluorocarbons (CFC) and chlorofluorobromocarbons (halons). An important ozone loss cycle involves the coupling of chlorine and bromine chemistry in the upper atmosphere in

[1] Permanent address: Department of Physics and Astrophysics, University of Delhi, Delhi 110007, India.

which OClO plays a key role. The OClO molecule is stratospherically important due to its abundance during polar nights. It is formed by the bimolecular reaction:

$$\mathrm{BrO} + \mathrm{ClO} \rightarrow \mathrm{Br} + \mathrm{OClO}. \tag{1}$$

OClO is therefore used as an indicator for monitoring the stratospheric bromine budget.

Although the spectroscopy of OClO has been extensively studied, the interaction of electrons with the OClO molecule remains poorly characterized. In previous studies, we reported the first data on electron-impact scattering from the ClO molecule (Baluja *et al* 2000) and from the Cl_2O molecule (Baluja *et al* 2001). These data were generated using the *R*-matrix method employing the UK polyatomic *R*-matrix code (Morgan *et al* 1997, 1998). In the present paper, we extend this study to the OClO molecule.

Experimental work on OClO is difficult because it is explosive and inherently unstable, and must be handled with caution. The optical absorption of OClO has been studied extensively. For example, Wahner *et al* (1987) and Hubinger and Nee (1994) recorded the absorption spectrum in the energy range 2.5–4.4 eV where the photoabsorption cross section is dominated by the transition from the ground state $\mathrm{X}\,^2\mathrm{B}_1$ to the excited state $\mathrm{A}\,^2\mathrm{A}_2$. These optical absorption measurements were subsequently extended up to 12.5 eV using synchrotron electron energy-loss spectroscopy (Davies *et al* 1995). Electron-impact experiments include the study of dissociative electron attachment of Marston *et al* (1998) and Senn *et al* (1999) for electron energies up to 10 eV. These experiments revealed the presence of collision thresholds which may be ascribed to either shape or Feshbach resonances which were apparent at about 0, 0.7, 4.3, 6 and 8 eV.

Total cross sections for the scattering of electrons from OClO have been reported by Gulley *et al* (1998) in the electron energy range from 9 meV to 10 eV. At very low energies, their cross sections show structure which is probably due to rotationally inelastic scattering. There was a sharp minimum in the cross section at 38 meV and a subsequent maximum at electron-impact energies between 55 and 60 meV. These results also indicate a broad shoulder between 2 and 6 eV. However, the experiments of Gulley *et al* were later found to contain a strong residual due to the contaminant Cl_2, hence these cross sections were remeasured by Field *et al* (2000) with a purity level of OClO exceeding 90%. The new cross sections are significantly larger than the previous results. Cross sections for backward scattering of electrons from OClO were also reported in the range 20–500 meV. The ratio of the backward to the integral cross section is a qualitative measure of the efficiency of electron attachment. The backward scattering data indicate that dissociative attachment at low energies occurs through p-wave attachment. Other electron collision studies involving electron-impact ionization (O'Connor *et al* 1998, Muigg *et al* 2001) have been reported recently.

The open-shell nature of many of the Cl_xO_y compounds make them difficult systems to treat theoretically. Electron correlation plays an important role in these systems, not only for characterizing the ground state wavefunction, but also the many low-lying excited states which significantly affect low-energy electron collisions. Since OClO is an open-shell system, electron correlation plays a dominant role in determining the transition energies and transition moments among various electronic states.

In this paper we report the first electron collision calculations on OClO. These calculations are performed using the UK polyatomic *R*-matrix code (Morgan *et al* 1997, 1998), taking particular advantage of this method to give a good representation of the electron correlation in several excited states of the molecule (Tennyson 1996a).

2. Method

2.1. General considerations

The R-matrix method (Burke and Berrington 1993) divides configuration space into two regions. In the inner region, here defined by a sphere of radius 10 a_0 centred at the OClO centre of mass, the wavefunction is written using the configuration-interaction (CI) expression

$$\Psi_k = \mathcal{A} \sum_{ij} a_{ijk} \phi_i^N \eta_{ij} + \sum_j b_{jk} \phi_j^{N+1} \tag{2}$$

where ϕ_i^N represents the ith state of the N-electron target, η_{ij} is a function representing the continuum electron and $\mathcal{A}$ is an antisymmetrization operator. The continuum functions are the only functions with amplitude on the R-matrix boundary. The second sum in (2) comprises configurations composed of short-range functions. To obtain reliable results it is important to maintain a balance between the N-electron target representation, ϕ_i^N, and the $(N + 1)$-electron scattering wavefunction. The choice of appropriate ϕ_j^{N+1} is crucial in this (Tennyson 1996b). Coefficients a_{ijk} and b_{jk} are variational parameters determined as a result of the matrix diagonalization.

Inside the R-matrix sphere full electron–electron and exchange interactions are modelled explicitly. Outside the sphere, only long-range multipolar interactions between the scattering electron and the various target states are included. OClO is a strongly dipolar system which has to be taken into account both by propagating the R-matrix to large distance, 50 a_0 in this paper, and by considering convergence with respect to the partial-wave expansion used for the continuum orbitals, η_{ij}.

2.2. Target states

The equilibrium structure of OClO was determined by Flesch *et al* (1993). The OClO molecule is bent and belongs to the C_{2v} symmetry group. At the equilibrium geometry, the Cl–O bond length is 1.471 Å and the angle OClO is 117.5°. These parameters are used in the present calculations.

The OClO molecule is rich in electrons. Its electronic ground state configuration has been established through optical absorption studies (Peterson and Werner 1992, Flesch *et al* 1993). There are 14 core electrons and 19 valence electrons. The core consists of doubly occupied $1a_1$, $2a_1$, $3a_1$, $4a_1$, $1b_1$, $1b_2$ and $2b_2$ molecular orbitals. The 19 valence electrons are distributed in 10 molecular orbitals of type $5a_1$, $3b_2$, $6a_1$, $7a_1$, $4b_2$, $2b_1$, $5b_2$, $8a_1$, $1a_2$ and $3b_1$. For the ground state all molecular orbitals up to $1a_2$ are doubly occupied giving the state designation X $^2B_1$. The first three electronic excited states are formed in which one of the electrons from the molecular orbitals $1a_2$, $8a_1$ or $5b_2$ is promoted to the $3b_1$ molecular orbital, yielding the state designations $1\ ^2A_2$, $1\ ^2A_1$ and $1\ ^2B_2$, respectively, for the three lowest electronic excited states. Of these, state $1\ ^2A_2$ is the atmospherically most important. Its excitation gives rise to an intense UV/visible band around 3.5 eV (Peterson and Werner 1992). The state $1\ ^2A_1$ has a low oscillator strength and is possibly masked by $1\ ^2A_2$ in the absorption spectrum.

Previous theoretical work on the OClO spectrum includes a restricted Hartree–Fock calculation (RHF) (Gole 1980) and a multireference configuration-interaction (MRCI) calculation (Peterson and Werner 1992) of its four low-lying electronic states. In the MRCI calculation (Peterson and Werner 1992) for the four lowest electronic states, the one-particle basis set employed was the standard correlation consistent polarized quadruple zeta set of Dunning (1989) for oxygen and a primitive set of Partridge (1987) augmented with a 3d2f

Table 1. Vertical energy excitations (in eV) for the OClO target states generated using a CASCI model at the experimental geometry of the ground state. Also given are the dominant configuration of each state, the number of configurations, N, in the CAS and the theoretical values of Peterson and Werner (1992).

			Vertical excitation energies	
State	Configuration	N	This work	Peterson and Werner (1992)
X $^2B_1$		473	0	
1 $^2A_1$	$8a_1^{-1}3b_1^2$	477	2.96	3.15
1 $^2B_2$	$5b_2^{-1}3b_1^2$	477	2.99	3.20
1 $^2A_2$	$1a_2^{-1}3b_1^2$	463	3.44	3.66
1 $^4B_2$	$1a_2^{-1}3b_19a_1$	258	6.52	6.82
1 $^4A_2$	$6b_2^{-1}3b_19a_1$	246	6.87	7.96
1 $^4A_1$	$5b_2^{-1}3b_19a_1$	246	7.03	8.08
1 $^4B_1$	$8a_1^{-1}3b_19a_1$	258	8.21	8.27

polarization set for chlorine. The MRCI calculations were extended (Peterson and Werner 1996) to investigate the potential energy surfaces involved in the photodissociation of OClO to Cl + O_2.

Our calculations on OClO used the double zeta plus polarization Gaussian basis sets of Dunning and Hay (1977) and Magnusson and Schaefer (1985). We used the SCF molecular orbitals of the ground state in our configuration-interaction calculations of all four states which are included in the scattering calculation. In our target state calculations, in addition to the seven core orbitals three further molecular orbitals $5a_1$, $6a_1$ and $3b_2$ were also frozen in their SCF orbitals. The reduced active space did not make any significant changes to the total energies of the target states. In all of our calculations we have employed this model which comprises 20 frozen electrons and 13 valence electrons distributed according to ($7a_1$, $8a_1$, $9a_1$, $2b_1$, $3b_1$, $4b_2$, $5b_2$, $6b_2$, $1a_2$)[13]. We refer to this model as a complete active space configuration-interaction (CASCI) model. Our SCF calculations indicate that the highest occupied molecular orbital is $3b_1$ with a binding energy of −6.14 eV. The lowest unoccupied molecular orbital is $9a_1$ with energy +4.72 eV and the next unoccupied orbital is $6b_2$ with energy +5.36 eV. All three excited electronic states included in our calculations arise due to the promotion of one electron from one of the three valence molecular orbitals $5b_2$, $8a_1$ and $1a_2$ to the already singly occupied molecular orbital $3b_1$. Table 1 presents vertical excitation energies for the states considered in our calculation. These are in good agreement with the calculations of Peterson and Werner (1992). The experimentally determined excitation energy of the atmospherically most important state 1 $^2A_2$ centred around the 3.5 eV band is in excellent agreement with our value of 3.44 eV.

Our CASCI model gives a dipole moment of 2.293 D and quadrupole moments $Q_{20} = -1.755$ and $Q_{22} = -3.898$ au at the equilibrium geometry of OClO molecule. This value of dipole moment is in reasonable agreement with the value 2.084 D calculated by McGrath *et al* (1990) who used a polarized split-valence basis set using second-order Moller–Plesset (MP2) perturbation theory. The difference of about 10% between the two theoretical values is due to different basis sets, different amounts of correlation and a slight difference in the equilibrium geometries involved. These theoretical values are higher than the two measured values of the dipole moment of OClO by Tolles *et al* (1962) using the Stark effect with a value of 1.784 D, and by Tanaka and Tanaka (1983) using laser Stark spectroscopy with a value of 1.792 D.

2.3. Scattering model

Our best model used the eight target states given in table 1 in the close-coupling expansion (2). We also performed test scattering calculations in the static-exchange (SE) and static-exchange with polarization (SEP) models. All calculations were performed for singlet and triplet states with A_1, B_1, B_2 and A_2 symmetries. In these calculations, the continuum orbitals were represented by Gaussians centred at the molecule centre of gravity. For this the orbitals of Sarpal *et al* (1996) were used. All calculations were performed for continuum orbitals up to f ($l \leqslant 3$). These continuum orbitals were orthogonalized to the target orbitals retained in the calculation and those with an overlap of less than 2×10^{-7} were removed (Morgan *et al* 1997).

Calculations, from SE upwards, were performed to test the stability of our model and assign resonances. These calculations included some with hand-picked configurations which allowed us to give orbital designations to the resonances we found and to probe the cause of pseudo-resonances which are high-energy artefacts of any truncated coupled-channels calculation.

One advantage of the CAS CI target model employed here is that the ϕ_j^{N+1} functions, see (2), can be defined in a fashion which retains the balance of the calculation (Tennyson 1996b). All $(N + 1)$-electron configurations of the appropriate total symmetry given by $(\text{core})^{20}$ $(7a_1, 8a_1, 9a_1, 2b_1, 3b_1, 4b_2, 5b_2, 6b_2, 1a_2)^{14}$ were retained. This means that 20 electrons are frozen in the core and 14 electrons are free to move among the molecular orbitals as given within the brackets.

3. Results

3.1. Anionic bound state

Our CI model gives a value of 2.293 D for the dipole moment of OClO which is strong enough to support a bound state of the anion. All the scattering models except the SE model found a bound state of OClO with $^1A_1$ symmetry. The energy of the state was determined using our bound state detecting code BOUND (Sarpal *et al* 1991). Our best model gave OClO an electron affinity of 1.547 eV at its equilibrium geometry. The inclusion of rotational motion (Crawford and Garrett 1977) will reduce the anionic binding energy, but the strong dipolar nature of OClO will keep the anionic state intact.

We also performed a standard bound state quantum chemistry calculation on the anionic state of $^1A_1$ symmetry using the same orbitals and model employed for the scattering calculations. This calculation gave a very similar result, an OClO electron affinity of 1.558 eV at the equilibrium geometry. From photoelectron spectroscopy (Gilles *et al* 1992) the adiabatic electron affinity of OClO is 2.14 eV. Given the difference between vertical and adiabatic binding energies these results are consistent with each other. However, we note that our SEP model only yields a weak anionic binding energy of 0.52 eV.

3.2. Elastic scattering

We carried out the scattering calculations in four models. These are SE, SEP, four- and eight-state models. Our best model is the eight-state model. In this model, 16 channels are coupled for singlet scattering symmetries and 32 channels for triplet symmetries. The number of configuration state functions for each triplet and singlet scattering symmetry is around 5900 and 3900, respectively. Due to the presence of long-range dipole interaction, the elastic cross section is formally divergent in the fixed-nuclei approximation. However, the elastic scattering data can be exploited to yield rotationally summed cross sections. Due to the permanent nature

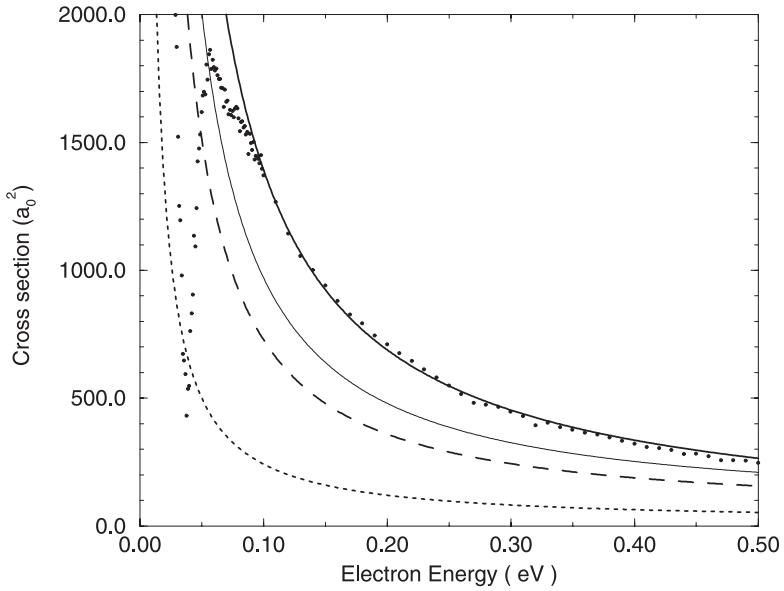

Figure 1. Eight-state R-matrix elastic (up to the f partial-wave) and rotational cross sections for electron impact on the $X\,^2B_1$ state of OClO: dotted curve, singlet symmetries, elastic cross sections; broken curve, triplet symmetries, elastic cross sections; thin full curve, singlet + triplet symmetries, elastic cross sections; full curve, Born-corrected summed rotational cross section; dots, experiment, Field *et al* (2000).

of the dipole moment of the OClO molecule, a very large number of partial waves must be taken into account to obtain converged results. States with $l \geqslant 4$ omitted from our calculations were allowed for by using the Born approximation (Gianturco and Jain 1986). The rotational spectrum of OClO has been analysed in great detail by Muller *et al* (1997). The rotational constants for OClO at the equilibrium geometry are 1.737 24, 0.331 98 and 0.278 00 cm^{-1} (Muller *et al* 1997). The OClO molecule is an asymmetric top but has one moment of inertia considerably greater than either of the other two. The value of the asymmetry parameter is -0.926, which is close to -1, and therefore to a good approximation it may be treated as a prolate symmetric top.

Figure 1 presents integral rotationally inelastic scattering cross sections for our eight-state model and compares these with the experiment (Field *et al* 2000) for electron energies up to 500 meV. Since low-energy scattering of electrons from polar molecules is largely determined by electron–permanent-dipole interaction, we have used the experimental value 1.792 D (Tanaka and Tanaka 1983) in the outer region. Use of the larger theoretical dipole moment in the outer region gives slightly higher cross sections for energies up to 300 meV, above which there is hardly any difference. Figure 1 also shows the contribution of summed singlet and summed triplet scattering symmetries up to f partial waves. Our Born-corrected cross sections are in good agreement with the experimental values at energies above 100 meV, but do not reproduce the sharp minimum observed in the cross section below this. If this minimum is due to interference effects between rotational excitation and other channels, as suggested by Field *et al*, then it could only be modelled by a more sophisticated treatment of the rotational excitation problem than we employ here.

The main feature in the elastic cross section is the presence of resonances in the $^1B_1$, $^3B_1$, $^1A_2$ and $^3A_2$ symmetries. In figure 2, we present cross sections for the $^3B_1$ resonance in the

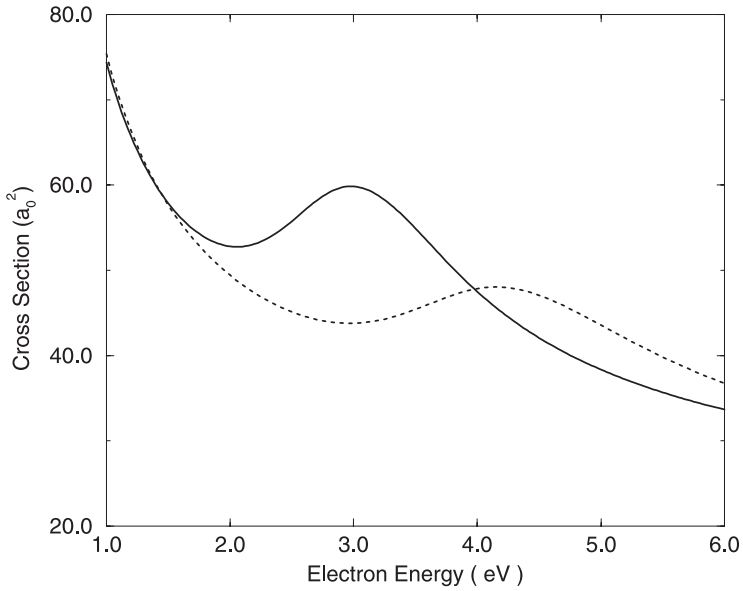

Figure 2. $^3B_1$ contribution to the total cross section including the Born correction, illustrating the role of the $^3B_1$ shape resonance: full curve, eight-state *R*-matrix; dotted curve, four-state *R*-matrix.

four- and eight-state models. For the eight-state model the $^3B_1$ feature is a shape resonance located at 2.961 eV with a width of 0.843 eV. For the four-state model, this resonance lies at a higher energy of 4.011 eV, i.e. above the doublet excited states. As the number of states included in the calculation increases, the position of the resonance shifts to a lower energy and becomes narrower. This is due to the increased attractive polarization potential experienced by the scattering electron.

The $^1B_1$ resonance in the eight-state model is located at 5.750 eV with a width 1.405 eV. For the four-state model this resonance position moves to a higher energy at 5.843 eV and is even broader than the eight-state result. The $^3A_2$ resonance in the eight-state model is located at 7.22 eV with a width 1.50 eV, while the corresponding values for the $^1A_2$ resonance are 8.06 and 2.72 eV. These broad resonance features are present even in the SE model, provided we use a complete active space CI target wavefunction, and therefore are probably best described as shape resonances. Our previous study on Cl_2O^- (Baluja *et al* 2001) also found a number of shape resonances which therefore seem to be a particular feature of these electron-rich oxides of chlorine.

The dominant configuration of $^1B_1$ and $^3B_1$ resonances is $3b_1 9a_1$; it should be noted that the $9a_1$ orbital is substantially of p character. The dominant configuration of $^1A_2$ and $^3A_2$ shape resonances is $3b_1 6b_2$. The resonant positions at 5.750 and 2.961 eV correlate approximately with maxima in the cross sections in the dissociative electron attachment observed by Marston *et al* (1998) and Senn *et al* (1999), which lie near 6 and 4.3 eV, respectively.

3.3. Inelastic cross sections

Figures 3–5 present OClO electron-impact electronic excitation cross sections from the ground state to the doublet excited states included in the calculations. According to the symmetry group

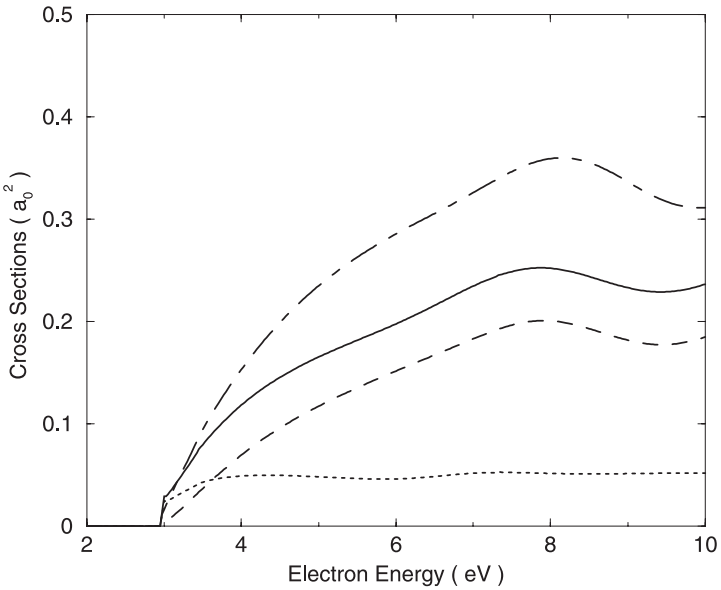

Figure 3. Electron-impact excitation of transition X $^2B_1$–1 $^2B_2$ of OClO. Full curve, eight-state R-matrix cross sections; chain curve, four-state R-matrix cross sections; dotted curve, eight-state R-matrix cross sections for triplet symmetries; broken curve, eight-state R-matrix cross sections for singlet symmetries.

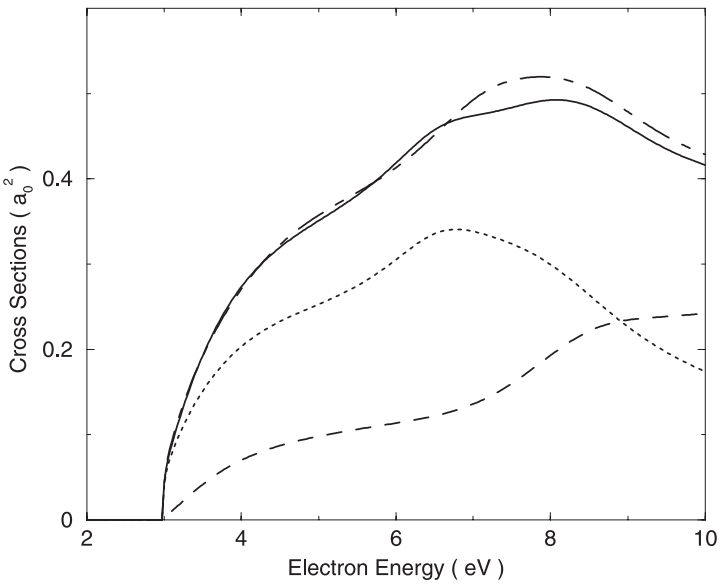

Figure 4. Electron-impact excitation of transition X $^2B_1$–1 $^2A_1$ of OClO. Full curve, eight-state R-matrix cross sections; chain curve, four-state R-matrix cross sections; dotted curve, eight-state R-matrix cross sections for triplet symmetries; broken curve, eight-state R-matrix cross sections for singlet symmetries.

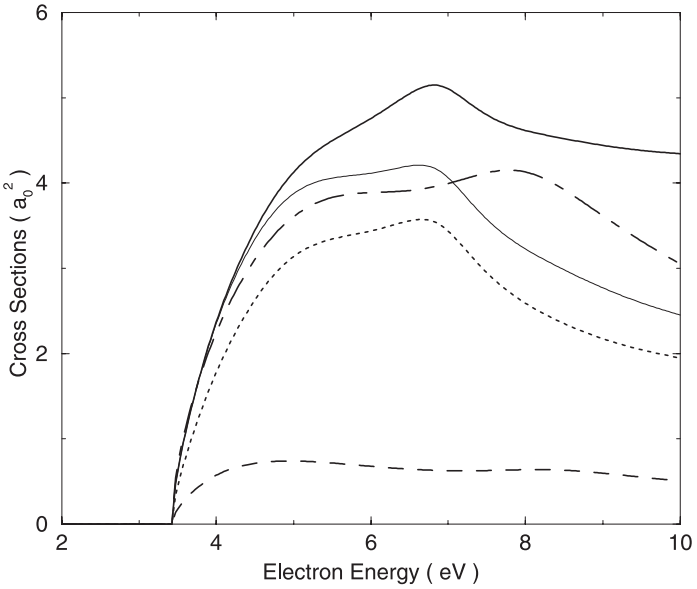

Figure 5. Electron-impact excitation of transition X $^2B_1$–1 $^2A_2$ of OClO. Full curve, Born-corrected eight-state *R*-matrix cross sections; thin full curve, uncorrected eight-state *R*-matrix cross sections; chain curve, four-state *R*-matrix cross sections; dotted curve, eight-state *R*-matrix cross sections for triplet symmetries; broken curve, eight-state *R*-matrix cross sections for singlet symmetries.

and the optical selection rules, transitions from the ground state to all doublet excited states are dipole allowed except those to the $^2B_2$ state.

The first excited state has symmetry $^2B_2$. The corresponding integrated cross sections are shown in figure 3 for our four- and eight-state calculations. The contributions of singlet and triplet symmetries for our best model are shown. The most significant contribution comes from $^1A_1$ symmetry and the next important contribution is from $^1B_2$ symmetry. The contribution from $^1A_2$ and $^1B_1$ symmetries is almost negligible. The triplet symmetries $^3B_2$ and $^3A_1$ dominate over the remaining triplets. For this optically forbidden transition, the total contribution from the singlet symmetries is much more than the total contribution from the triplet symmetries. The summed triplet cross section is almost flat over the entire energy range. In contrast, the summed singlet cross sections show a peak in the cross section at 8 eV which is due to the combined effect of $^1B_2$ and $^3B_2$ symmetries. The cross sections in our best model are lower in magnitude than our four-state model due to the loss of flux into other accessible channels. The peak around 8 eV is shifted to a slightly higher energy when the quartet states are excluded from the scattering calculation.

The cross section for exciting the second, $^2A_1$, state is shown in figure 4. This is a dipole-allowed transition but is weak with a transition moment of 0.0821 au. The $^2B_2$ and $^2A_1$ states are almost degenerate but the integrated cross sections for exciting the $^2A_1$ state are higher than the excitation of the $^2B_2$ state due to the former state being optically allowed. We have shown the contribution of singlet and triplet symmetries for our best model. The triplet contribution is more than the corresponding contribution from singlets up to 9 eV. Among the singlets, the $^1A_1$ symmetry is dominant. The $^1B_2$ symmetry begins to contribute beyond 8 eV, the remaining singlets have a negligible effect on the cross section. The cross section due to $^3A_1$ symmetry rises sharply at the threshold and has a peak around 6.5 eV. There is also a peak in

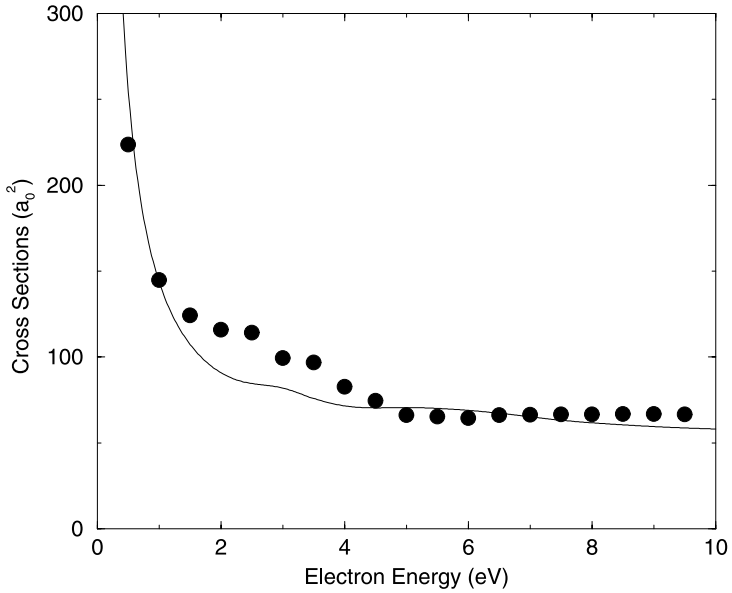

Figure 6. Total (elastic + excitation) cross section for electron impact of OClO. Full curve: eight-state *R*-matrix cross sections; circles: rescaled experiment of Gulley *et al* (1998), see text for details.

the cross section in the $^3B_2$ symmetry at about 8 eV. The net effect of all the singlets and triplet symmetries is to produce a hump around 8 eV. The cross sections for our eight-state model are lower than the four-state results above the threshold of the first excited quartet state.

In figure 5, we have displayed the cross sections for the excitation of $^2A_2$ state. This is a dipole-allowed transition with a transition moment of 0.6092 au. The structure in the four- and eight-state models arises in the $^3A_2$ symmetry. The peak in the best model is shifted by almost 1 eV when quartets are included in the scattering calculation with respect to the four-state model which only includes doublet target states. To obtain converged cross sections, the contribution of partial waves higher than f-wave have been accounted for through closure relations (Crawford and Dalgarno 1971) in the Born approximation. The uncorrected and Born-corrected cross sections for our eight-state model are shown. Away from threshold, the contribution of higher partial waves are quite important for this strong dipole-allowed transition. The cross section due to singlets rises from threshold and then becomes almost constant beyond 4 eV. The cross section due to $^3A_2$ symmetry is very prominent and contributes almost half to the integrated cross section at the peak. All the remaining triplets contribute significantly. Among the singlets, the contribution of $^1A_2$ symmetry is almost half of the summed cross section for singlets.

Finally, in figure 6 we present total (elastic plus excitation) cross sections for the eight-state model and compare these with the (rescaled) experimental data of Gulley *et al* (1998). Due to the presence of an impurity in the OClO sample, the measured values for the total scattering cross sections were found to be too low. Therefore, we have renormalized the data to the new, high-purity values of Field *et al* (2000) at 0.5 eV. The result is good agreement between both the magnitude and shape of the theoretical and experimental results. In particular, we note that our calculations reproduce the broad shoulder between 2 and 6 eV in the experimental results.

4. Conclusions

This is the first theoretical study of electron impact on the open-shell radical OClO. Our calculations predict a bound anionic state and four shape resonances which correlate with maxima observed in the dissociative electron attachment cross sections. Our calculations also agree quantitatively with the total cross sections in the several hundred meV range and reproduce the salient features such as the presence of a shoulder in the few eV range. This is encouraging and suggests that the results reported by us previously on ClO (Baluja *et al* 2000) and Cl_2O (Baluja *et al* 2001), for which there were no experimental data available for comparison, should provide accurate predictions above the low-energy region. However, our calculations do not reproduce the sharp minima observed in the cross section at electron energies below 100 meV; such behaviour can probably only be modelled with a much more sophisticated treatment of the electron-impact rotational excitation problem than that used here.

Acknowledgments

This work was supported by the UK Engineering and Physical Sciences Research Council via a visiting Fellowship for KLB and other grants.

References

Baluja K L, Mason N J, Morgan L A and Tennyson J 2000 *J. Phys. B: At. Mol. Opt. Phys.* **33** L677
——2001 *J. Phys. B: At. Mol. Opt. Phys.* **34** 2807
Burke P G and Berrington K A (ed) 1993 *Atomic and Molecular Processes: an R-Matrix Approach* (Bristol: IOP Publishing)
Cicerone R J 1987 *Science* **237** 35
Crawford O H and Dalgarno A 1971 *J. Phys. B: At. Mol. Phys.* **13** 494
Crawford O H and Garrett W R 1977 *J. Chem. Phys.* **66** 4968
Davies J A, Mason N J, Marston G and Wayne R P 1995 *J. Phys. B: At. Mol. Opt. Phys.* **28** 4179
Dunning T H 1989 *J. Chem. Phys.* **90** 1007
Dunning T H and Hay P J 1977 *Methods of Electronic Structure Theory* vol 2, ed H F Schaefer (New York: Plenum)
Field D, Jones N C, Gingell J M, Mason N J, Hunt S L and Ziesel J P 2000 *J. Phys. B: At. Mol. Opt. Phys.* **33** 1039
Flesch R, Ruhl E, Hottmann K and Baumgartel H 1993 *J. Phys. Chem.* **97** 837
Gianturco F A and Jain A 1986 *Phys. Rep.* **143** 347
Gilles M K, Pollak M L and Lineberger W C 1992 *J. Chem. Phys.* **96** 8012
Gole J L 1980 *J. Phys. Chem.* **84** 1333
Gulley R J, Field T A, Steer W A, Mason N J, Lunt S L, Ziesel J P and Field D 1998 *J. Phys. B: At. Mol. Opt. Phys.* **31** 5197
Hubinger S and Nee J B 1994 *Chem. Phys.* **181** 247
Magnusson E and Schaefer H F 1985 *J. Chem. Phys.* **83** 5721
Marston G, Walker I C, Mason N J, Gingell J M, Zhao H, Brown K L, Motte-Tollet F, Delwiche J and Siggel M R F 1998 *J. Phys. B: At. Mol. Opt. Phys.* **31** 3387
McGrath M P, Clemitshaw K C, Rowland F S and Hehre W J 1990 *J. Phys. Chem.* **94** 6126
Morgan L A, Gillan C J, Tennyson J and Chen X 1997 *J. Phys. B: At. Mol. Opt. Phys.* **30** 4087
Morgan L A, Tennyson J and Gillan C J 1998 *Comput. Phys. Commun.* **114** 120
Muigg D, Denifel G, Stamatovic A, Mason N J and Mark T D 2001 *J. Chem. Phys.* at press
Muller H S P, Sorensen G O, Birk M and Friedl R R 1997 *J. Mol. Spectrosc.* **186** 177
O'Connor C, Tafadar T and Price S D 1998 *J. Chem. Soc. Faraday Trans.* **94** 1797
Partridge H R 1987 *Nasa Technical Memorandum* 89449
Peterson K A and Werner H J 1992 *J. Chem. Phys.* **96** 8948
——1996 *J. Chem. Phys.* **105** 9823
Rowland F S 1991 *Ann. Rev. Phys. Chem.* **42** 731
Sarpal B K, Branchett S E, Tennyson J and Morgan L A 1991 *J. Phys. B: At. Mol. Opt. Phys.* **24** 3685

Sarpal B K, Pfingst K, Nestmann B M and Peyerimhoff S D 1996 *J. Phys. B: At. Mol. Opt. Phys.* **29** 857
Senn G, Drexel H, Marston G, Mason N J, Mark T D, Meinke M, Schamle C, Tageder P, Ruhl E and Illenberger E 1999 *J. Phys. B: At. Mol. Opt. Phys.* **32** 3615
Tanaka K and Tanaka T 1983 *J. Mol. Spectrosc.* **98** 425
Tennyson J 1996a *J. Phys. B: At. Mol. Opt. Phys.* **29** 1817
——1996b *J. Phys. B: At. Mol. Opt. Phys.* **29** 6185
Tolles W M, Kinsey J L, Curl R F Jr and Heidelberg R F 1962 *J. Chem. Phys.* **37** 927
Wahner A, Tyndall G S and Ravishankara A R 1987 *J. Phys. Chem.* **91** 2734